Analysis and Design of Reconfigurable Multiband Mismatch-Resilient Quasi-Balanced Doherty Power Amplifier for Massive MIMO Systems

Haifeng Lyu, *Graduate Student Member, IEEE*, and Kenle Chen, *Senior Member, IEEE*

***Abstract*— A novel power amplifier (PA) with wide bandwidth and load mismatch resilience is presented based on the quasi-balanced Doherty PA (QB-DPA) architecture. By reconfiguring the parallel/series QB-DPA operation modes with the nominal/exchanged biasing alternation and control of phase dispersion, the proposed QB-DPA topology can overcome the bandwidth limitations and ensure a standard Doherty profile and high efficiency and linearity against dynamic load mismatch over the operational bandwidth. Based on the theoretical analysis, a design guidance of output matching topology on phase offset implementation is presented. As a proof of concept, a physical prototype is demonstrated targeting for 1.7–2.7-GHz bandwidth. The developed QB-DPA achieves an efficiency of 56%–78% at OP_{1dB} and 47%–71% at 6-dB output back-off (OBO) over the in-band operation with 50-Ω load. Through reconfiguration (parallel/series mode for mismatch recovery and nominal/exchanged biasing for bandwidth extension), the developed QB-DPA demonstrates significantly improved OP_{1dB} variation both at center frequency 2.1 GHz and edged-frequency 1.7 and 2.6 GHz at 2:1 voltage standing wave ratio (VSWR) over 360° phase span. In modulated measurement using 20-MHz long-term evolution (LTE) signals, >44.5% average efficiency and <−30.9-dBc adjacent channel power ratio (ACPR) are obtained across the wide bandwidth at matched-load condition. More importantly, for VSWR 2:1 circle, the high linearity [<5.3% error vector magnitude (EVM)] and average efficiency (>38.1%) can be experimentally maintained through reconfigurations.**

***Index Terms*— Doherty power amplifier (DPA), linearity, load mismatch, multiband reconfigurable.**

I. Introduction

With the insatiable demand for high-speed wireless data transmission, the wideband and spectrally-efficient modulation schemes are ubiquitously adopted in modern wireless systems. However, the high peak-to-average power ratio (PAPR) caused by the increasing number of subcarriers and high modulation order in these advanced schemes leads to the fact that power amplifiers (PAs) have to operate at a large power backed-off range most of the time. As a result, PA architectures with back-off efficiency enhancement are highly desired to amplify such high-PAPR signals. Moreover, with the proliferation of communication bands, the PAs are expected to support multiband/multimode operations to minimize the number of PAs in a wireless platform for sustainable cost and space at system level. Therefore, broadband and highly performance PA technologies are of crucial importance for next-generation wireless systems.

Meanwhile, to further enhance the spectral efficiency, array-based spatial multiplexing technique has been widely exploited in 5G base stations that leverages the spatial differences to enable concurrent transmission of multiple signals at the same frequency, also known as massive multiple-input multiple-output (MIMO). However, the high-density antenna array inevitably brings about strong mutual couplings between the colocated antennas due to the near field scattering (lattice spacing between elements) and limited isolation on substrate [1], [2], [3], [4], [5], [6]. Moreover, these couplings result in a high-speed antenna impedance variation as well as large voltage standing wave ratio (VSWR). Directly loaded by the antenna, the PAs in the array are load-pulled, and this load-pulling effect depends on both the scan angle and element location [7]. Consequently, the PAs can suffer from significant performance (e.g., efficiency, linearity, and OP_{1dB}) degradation, since the PA operation is governed by its loadline [8]. A more severe issue is the main beam distortion due to the accumulated PA nonlinearity among the array, and it leads to a major challenge for digital predistortion (DPD) that has to be applied at array level [9], [10], [11], [12].

To improve the Pas' performance under mismatch, antenna isolation has been applied to block the effect of antenna-impedance variation from PA for decades. However, the isolators/circulators, typically based on magnetic materials, are bulky, expensive, and lossy prohibiting the large-scale integration in a massive MIMO system. Passive tunable matching networks (TMNs) have been widely employed in handset devices to compensate for the dynamic load impedance [13], [14], [15], [16]. However, the TMNs are typically lossy and bulky since extra building blocks are requires, leading to a major difficulty for array-level integration. To solve this issue, a promising solution is to merge this tuning-based approach into the PA stage. In [17], a broadband Doherty-like PA through active load pulling to a multiport combiner

Manuscript received 25 February 2022; revised 5 May 2022; accepted 2 July 2022. Date of publication 24 August 2022; date of current version 5 October 2022. This work was supported in part by the National Science Foundation under Award 1914875. This article is an expanded version from the IEEE MTT-S International Conference on June 7, 2021 Atlanta, USA [DOI: 10.1109/TMTT.2022.3198437]. *(Corresponding author: Kenle Chen.)*

The authors are with the Department of Electrical and Computer Engineering, University of Central Florida, Orlando, FL 32816 USA (e-mail: haifeng@knights.ucf.edu; kenle.chen@ucf.edu).

Color versions of one or more figures in this article are available at https://doi.org/10.1109/TMTT.2022.3198437.

Digital Object Identifier 10.1109/TMTT.2022.3198437

is exploited to improve VSWR-related degradation at peak power. However, the presented architecture only exhibits Doherty-like performance across a narrow bandwidth with a 50-Ω load. More than 10% of power-added efficiency (PAE) and 2 dB of output power degradation are reported for a single-frequency operation over 4:1 VSWR circle. A coupler-based hybrid series/parallel reconfigurable Doherty PA (DPA) is presented in [18], which utilizes exchangeable gate biasing, tunable phase offset at input, and adjustable current weighting of main/auxiliary PAs to counteract the load mismatch. The demonstrated prototype achieves a wideband small-signal S_21 response at nominal load without large-signal and VSWR capability over the bandwidth. Very recent works [19], [20] based on load-dependent supply modulation adaption together with adjustable main-auxiliary phase offset also show a decent load insensitivity. Nevertheless, the realistic implementation of this approach requires extra dc–dc converters that may be challenging for integration into a massive array. Overall, while various techniques have been reported for PAs with tolerance to load mismatch, a systematic design methodology is still necessary for PA with sustainable high efficiency and linearity not only against a large variation range of load impedance but also over a broad bandwidth.

This article presents a novel wideband reconfigurable quasi-balanced DPA (QB-DPA). Compared with previous work [21], the proposed design for the first time shows that the QB-DPA is able to maintain a stable $OP_{1\,dB}$ as well as enhanced efficiency and linearity across 2:1 VSWR circle, and this operation can be seamlessly extended to a wide bandwidth through parallel/series reconfiguration and reciprocal biasing. Based upon the preliminary study in [22], this article significantly expands the conference paper in the following aspects. First, a generalized theory of QB-DPA is analytically established and extended by including the effects of transistor parasitics and matching network, and it is mathematically proved that a wideband back-off efficiency enhancement can be achieved through a proper control of the phase dispersion from the realistic parasitic and output-matching networks (OMNs). Second, a systematic design methodology is thoroughly explained in terms of matching topology selection and compensation for the parasitics. Third, a prototype design of a 1.7–2.7-GHz wideband mismatch-resilient QB-DPA is presented, which not only exhibits back-off efficiency enhancements with 50-Ω load but also achieves a first-ever wideband mismatch-resilient operation with <1.9-dB $OP_{1\,dB}$ fluctuation and >46% efficiency at $P_{1\,dB}$ under 2:1 VSWR. Furthermore, the measurement results using continuous-wave (CW) and modulated signals compare favorably with state-of-the-art for both nominal matched load and 2:1 VSWR [17], [18], [19], [20], [21], [23], which further demonstrate the effectiveness of proposed method and holds promising potential for application to array-based massive MIMO systems.

II. Mismatch-Resilient and Wideband Quasi-Balanced Doherty Theory

As illustrated in Fig. 1(a), the reconfigurable QB-DPA architecture is composed of main/auxiliary PAs and a output-coupler combiner with a 90° input phase shift between the

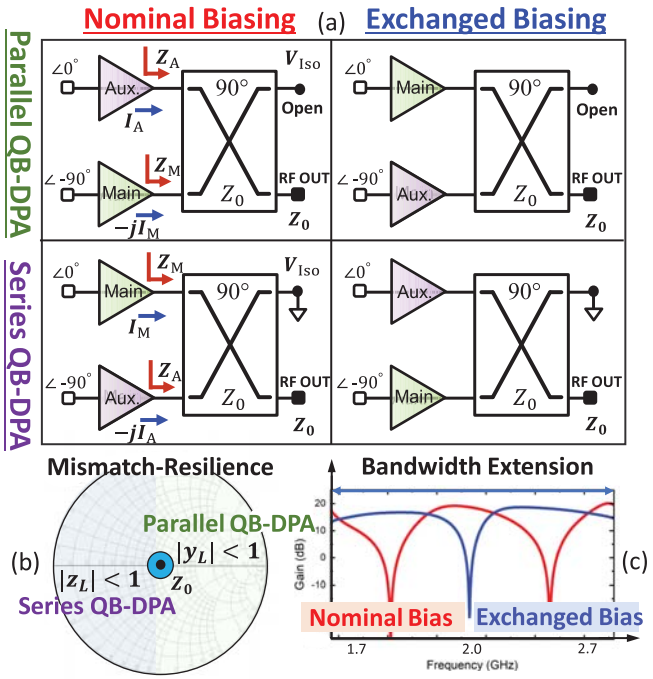

Fig. 1. Proposed wideband QB-DPA. (a) Circuits mechanism for parallel/series switching and nominal/exchanged biasing alteration, (b) operation division for parallel/series QB-DPA to recover mismatch, and (c) broadband realization with nominal/exchanged biasing.

two PAs. Unlike the unbalanced PA architecture in [24], where the back-off efficiency enhancement at 50-Ω load is realized through adjustment of the transistor's width ratio (transistor size) and output Lange coupler's coupling coefficient, the QB-DPA is theoretically equivalent to the classical DPA [21], [25], which is designed symmetrically with equal size of the main/aux. transistors and even 3-dB power splitter/combiner. By means of the role-exchange of PAs (different gate-bias settings) and swapping of open-/short-circuit loading of isolation port, the QB-DPA can maintain the $OP_{1\,dB}$, maximal achievable efficiency, and linearity against arbitrary variations of load impedance. To further extend this QB-DPA architecture to wideband operation, theoretical analysis considering transistors' parasitics and the effects of realistic matching networks is performed. Meanwhile, a reciprocal biasing scheme is proposed to overcome the bandwidth limitation due to the imperfections of realistic quadrature coupler.

A. Ideal Parallel and Series Quasi-Balanced Doherty PA for Mismatch Recovery

The theoretical analysis of Doherty load modulation (LM) through the quadrature coupler is performed based on the impedance matrix (Z-matrix) of coupler. As shown in Fig. 1(a), to obtain the LM of main and auxiliary amplifiers, the PAs are modeled as ideal voltage-controlled current sources applied to the respective ports of Z-matrix of quadrature coupler. For parallel QB-DPA depicted in Fig. 1(a), the isolation port is open circuited with voltage only, and the voltages and currents associated with the Z-matrix are

expressed as

$$\begin{bmatrix} V_0 \\ V_{\text{Iso}} \\ V_M \\ V_A \end{bmatrix} = \hat{\boldsymbol{Z}}_{\textbf{coupler}} \begin{bmatrix} I_0 \\ 0 \\ -jI_M \\ I_A \end{bmatrix} \tag{1}$$

where V_0 and I_0 denote the output voltage and current of the output port that is matched to Z_0 in nominal condition, and $V_{M/A}$ and $I_{M/A}$ represent the voltage and current of main/auxiliary amplifier, respectively. The matrix of $\hat{\boldsymbol{Z}}_{\textbf{coupler}}$ for the ideal 3-dB quadrature coupler matrix is given by

$$\hat{\boldsymbol{Z}}_{\textbf{coupler}} = Z_0 \begin{bmatrix} 0 & +j & -j\sqrt{2} & 0 \\ +j & 0 & 0 & -j\sqrt{2} \\ -j\sqrt{2} & 0 & 0 & +j \\ 0 & -j\sqrt{2} & +j & 0 \end{bmatrix}. \tag{2}$$

Consequently, the LM behaviors of main and auxiliary amplifiers in parallel mode are derived as

$$Z_{M_{\text{PL}}} = Z_0\left(2 + \frac{I_A}{I_M}\right) \quad \& \quad Z_{A_{\text{PL}}} = Z_0\frac{I_M}{I_A}. \tag{3}$$

For series QB-DPA mode shown in Fig. 1(a), the isolation port is short-circuited, and the main and auxiliary amplifiers are exchanged. Thereby, the voltage-current dependence with Z-matrix is rewritten as

$$\begin{bmatrix} V_0 \\ 0 \\ V_A \\ V_M \end{bmatrix} = \hat{\boldsymbol{Z}}_{\textbf{coupler}} \begin{bmatrix} I_0 \\ I_{\text{Iso}} \\ -jI_A \\ I_M \end{bmatrix}. \tag{4}$$

Nevertheless, the same (compared to the parallel mode) LM behaviors for main and auxiliary amplifiers are obtained

$$Z_{M_{\text{SE}}} = Z_0\left(2 + \tfrac{I_A}{I_M}\right) \quad \& \quad Z_{A_{\text{SE}}} = Z_0\tfrac{I_M}{I_A}. \tag{5}$$

The parallel/series QB-DPA behaves symmetrically at the nominal condition with matched load. More importantly, a complementary sensitivity under load mismatch can be utilized to create a mismatch-resilient QB-DPA as illustrated in Fig. 1(b). Given an arbitrary load admittance (impedance) of Y_L (Z_L), the LM of parallel/series QB-DPA can be calculated as

$$\begin{aligned} Z_{M_{\text{PL}}}(y_L) &= Z_0\frac{2y_LI_M + I_A}{I_M} \quad \& \quad Z_{A_{\text{PL}}} = Z_0\frac{I_M}{I_A} \\ Z_{M_{\text{SE}}}(z_L) &= Z_0\frac{2z_LI_M + I_A}{I_M} \quad \& \quad Z_{A_{\text{SE}}} = Z_0\frac{I_M}{I_A} \end{aligned} \tag{6}$$

in which $y_L(z_L)$ represents the normalized form of $Y_L(Z_L)$ to the matched admittance Y_0 (impedance Z_0). Further, the voltage expression at parallel/series mode of main/aux. PAs can be derived as below

$$\begin{aligned} V_{M_{\text{PL}}}(y_L) &= -j(2I_My_L - I_A)Z_0 \quad \& \quad V_{A_{\text{PL}}} = I_MZ_0 \\ V_{M_{\text{SE}}}(z_L) &= (2I_Mz_L - I_A)Z_0 \quad \& \quad V_{A_{\text{SE}}} = -jI_MZ_0. \end{aligned} \tag{7}$$

It is worthy to note that the main amplifier can suffer from substantial RF voltage swing that $|V_{M_{\text{PL/SE}}}| > |V_{\text{DD}}|$ (dc rail voltage), due to the excessively high $y_L > 1$ ($z_L > 1$) in parallel (series) mode in (7), which leads to severe nonlinearity, inefficiency, and reliability issues. Nevertheless, from Fig. 1(b), a nonvoltage clipping load-impedance region can be reconfigured for parallel mode at $|y_L| < 1$ (i.e., $|z_L| > 1$) and for series mode at $|z_L| < 1$ for VSWR tolerance, which indicates a full coverage of the entire Smith chart with a combined operation of two modes. Together with the fact that the auxiliary amplifier is naturally independent of the load in either mode, a completely clipping-free (mismatch-resilient) QB-DPA can be realized by leveraging the complementarity between parallel and series modes.

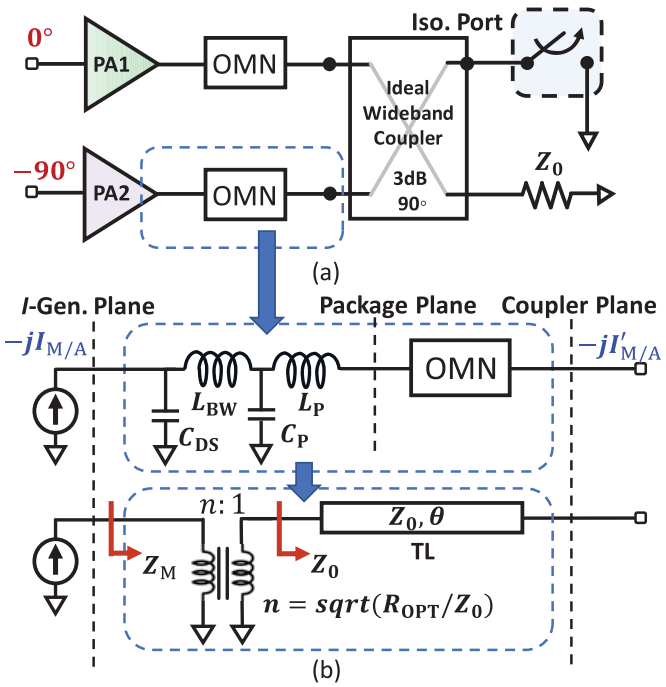

Fig. 2. (a) Proposed wideband QB-DPA OMN. (b) Equivalent OMN with ideal transformer and TL.

B. Effects of Transistor Parasitics and Matching Networks

The aforementioned generic QB-DPA architectures are based on ideal current sources directly coupled to the quadrature hybrid. Realistically, this model needs to be extended by including the effects of transistors' parasitics and OMNs, as is shown in Fig. 2. Each of the amplifiers is modeled as an ideal current source with parasitic network, which is connected to the quadrature coupler through a matching network. The combined passive network (parasitics + OMN) can be further modeled as an ideal transformer in conjunction with a transmission line (TL) of Z_0 characteristic impedance, offering functional equivalence in terms of impedance transformation and phase dispersion, as illustrated in Fig. 2(b).

To investigate the endurable phase θ variation range, theoretical study is performed on QB-DPA LM. This is particularly meaningful for wideband QB-DPA designs since the wideband OMNs usually have large phase dispersion. Ideally, the effective load impedance of the main amplifier in the back-off power region should be maintained to the desired value (i.e., $2Z_0$) for the matched load condition. In reality, due to the loading of peaking amplifier's OFF-state impedance, the back-off load impedance observed by main amplifier can

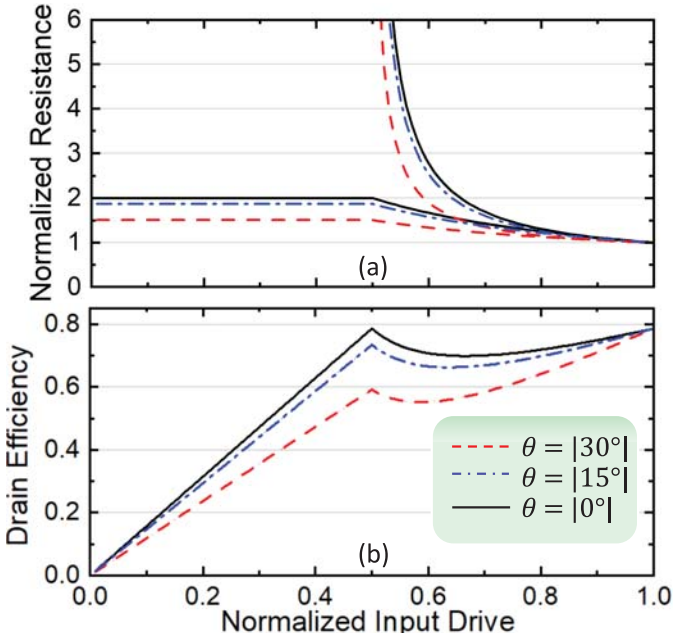

Fig. 3. Calculated QB-DPA behaviors due to the θ dispersion for (a) normalized resistance of Z_M and Z_A and (b) DE.

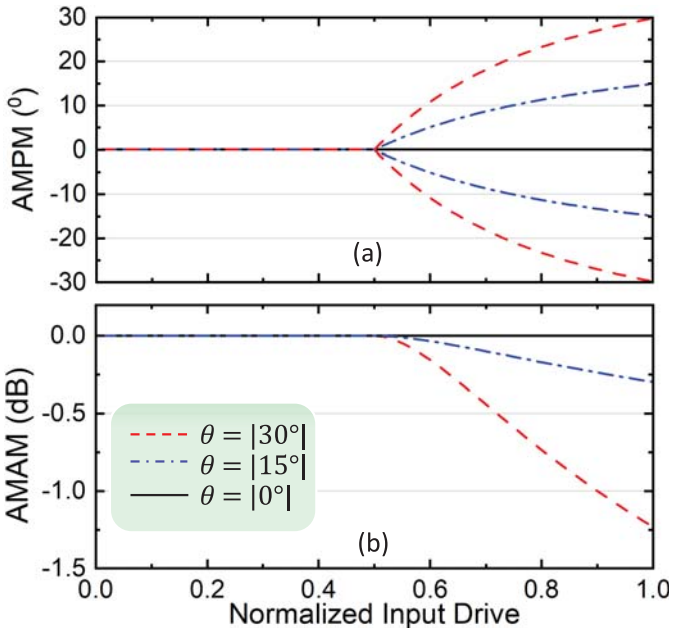

Fig. 4. Calculated QB-DPA behaviors due to the θ dispersion for (a) AM-PM and (b) AM-AM.

deviate from the optimal value, which leads to a distortion of LM behavior. To solve this issue, the OMN should ideally provide an opposing phase dispersion that compensates for the transistors' parasitic to maintain a desired Doherty profile. To mathematically evaluate the tolerable θ range, the ABCD matrix of the TL (Z_0, θ) in Fig. 2(b) is thus expressed as

$$\boldsymbol{A}_{\mathbf{TL}} = \begin{bmatrix} \cos\theta & jZ_0\sin\theta \\ j\sin\theta/Z_0 & \cos\theta \end{bmatrix}. \tag{8}$$

Subsequently, the ideal loadline seen at the intrinsic drain plane of main and auxiliary devices are derived through the interaction of output coupler and the TLs (Z_0, θ). Thus, by shifting the coupler matrix plane [26], (3) and (5) can be rederived as

$$Z_{M_{\mathrm{PL/SE}}} = n^2 Z_0 \left(2\cos\theta e^{-j\theta} + \frac{I_A}{I_M} e^{-j2\theta}\right) \tag{9}$$

$$Z_{A_{\mathrm{PL/SE}}} = n^2 Z_0 \left(\frac{I_M}{I_A} e^{-j2\theta} + 2j\sin\theta e^{-j\theta)}\right) \tag{10}$$

where n is the transformation coefficient for the ideal transformer in Fig. 2(b).

The fundamental RF power for main/auxiliary amplifier can be derived as

$$P_{M/A} = \frac{1}{2}\mathrm{Re}\left\{V_{M/A}[1]I^*_{M/A}[1]\right\} = \frac{1}{2}|I_{M/A}[1]|^2\mathrm{Re}\{Z_{M/A}\}. \tag{11}$$

Note that Z_M and Z_A expressed in (5) and (6) can be complex numbers. Then, the dc power is calculated by multiplying V_{DD} with the corresponding dc current extracted using the Class-B model [21], [28]. The normalized load resistance and efficiency are then calculated with a variation of θ. Fig. 3 indicates that once the phase variation due to the OMN and parasitics can be controlled within $\pm 15°$, above 70% back-off and 78% peak efficiency can be maintained with main and auxiliary devices both described using piecewise linear model, while a slightly distorted Doherty profiles are observed for the main and auxiliary PAs. Beyond the tolerable phase range of $\pm 15°$, a further degradation of Doherty performance occurs, which no longer provides sufficient efficiency enhancement at power back-off, e.g., $\theta = \pm 30°$ in Fig. 3. Moreover, the phase offset can be properly controlled through OMN design to generate a predistorted amplitude-to-phase (AMPM) response to compensate for the overall DPA's AMPM distortion due to LM [21], [29], as is shown in Fig. 4. Meanwhile, less than 0.3 dB of amplitude-to-amplitude (AMAM) distortion is achieved within $\pm 15°$ of θ variation, which is favorable for a linear DPA design. The above analysis applies for both parallel and series mode for their symmetry.

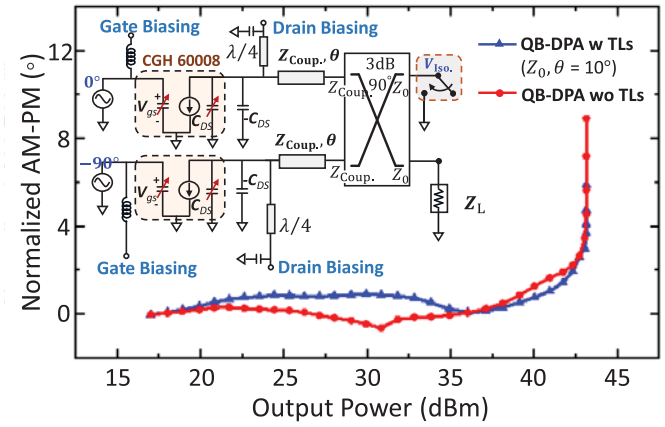

Fig. 5. Simulated AM-PM responses using emulated QB-DPA circuit model [27] for different values of phase dispersion.

The theoretical model is verified using an emulated circuit model of the QB-DPA as shown in Fig. 5. The development of such an emulated circuit model has been elaborated

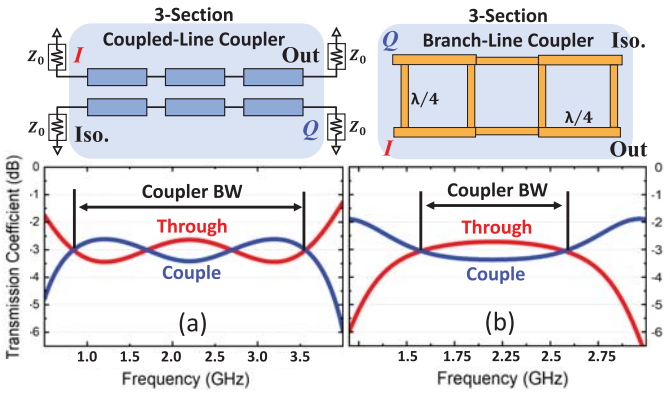

Fig. 6. Wideband coupler with transmission coefficients. (a) Coupled-line coupler. (b) Branch-line coupler.

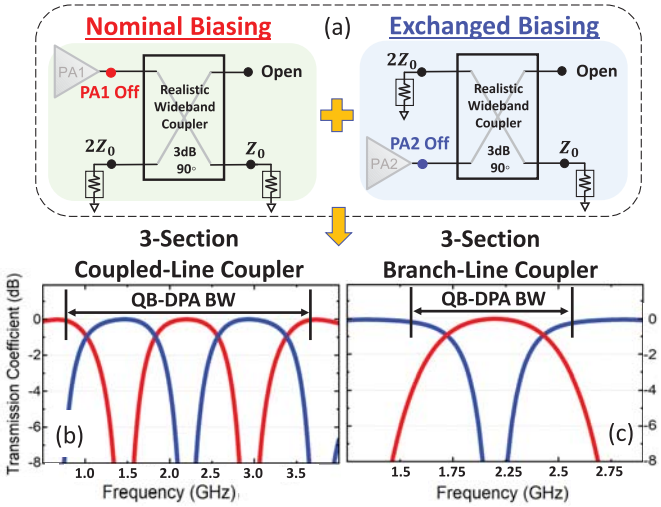

Fig. 7. Wideband QB-DPA at parallel mode. (a) Back-off power equivalent circuit with nominal/exchanged biasing, and bandwidth extension with combiner of (b) coupled-line coupler and (c) branch-line coupler.

in [27], in which bare-die transistor models are deembedded by incorporating static negative parasitic components, e.g., $-C_{\mathrm{DS}}$. The AMPM responses are simulated with different phase dispersion values. It can be seen that the generic QB-DPA with 0° phase dispersion (red curve in Fig. 5) can suffer from large AMPM distortion, especially during LM, which is primarily due to the nonlinear parasitics. Nevertheless, the AMPM (blue curve in Fig. 5) can be considerably linearized with proper phase dispersion from the main/auxiliary matching circuits, which generates a reverse AMPM distortion during LM to cancel the effect of nonlinear parasitics as indicated by Fig. 4(a).

Note that the quadrature coupler can be designed as an impedance transformer as depicted in Fig. 5 [30], and thus, simplified matching circuits can be utilized to maintain a low-phase dispersion (e.g., <15°) over a wide frequency range. As such, the QB-DPA architecture can be extended to wideband operation with minimal impact on the Doherty LM behavior and back-off efficiency enhancement. More importantly, the unique mismatch-resilient characteristic of QB-DPA can be effectively sustained over the same broad bandwidth through parallel/series reconfiguration.

C. Exchangeable Biasing for Bandwidth Extension

Another factor that restricts the bandwidth extension in this coupler-based QB-DPA architecture is the frequency-dependent variation of the wide-band coupler as Doherty combiner. Two widely used broadband couplers are analyzed to evaluate how the realistic coupler's frequency fluctuation impairs the DPA bandwidth. As shown the transmission (I) and coupling (Q) coefficients in Fig. 6(a), around 130% fractional bandwidth can be realized for a coupled-line coupler with four ports terminated to Z_0. However, in the parallel Doherty configuration, the main port connected to coupler is set to $2Z_0$, the auxiliary port is open-circuited at the back-off power region, and the isolation port is also open circuited, as shown in Fig. 7(a). The transmission coefficient between the main amplifier port and the output port is shown with the red curve in Fig. 7(b), which clearly indicates that the bandwidth is significantly compromised as compared to the original coupler. To fully utilize the achievable bandwidth of coupler, an approach of reciprocal biasing through exchanging the main/auxiliary settings is proposed. The transmission capacity can be restored with a complementary response over frequency as the blue curve illustrated in Fig. 7(a). With a combination of two biasing modes, the full coupler bandwidth can be exploited for Doherty design. The similar phenomenon is also observed for branch-line coupler, as presented in Figs. 6(b) and 7(c). Overall, by leveraging the exchangeable biasing, the frequency fluctuation due to the wideband coupler can be largely eliminated and then a broadband QB-DPA architecture is achieved. It is worthy to note that the above analysis is based on parallel QB-DPA, and it is also valid for series QB-DPA due to the symmetry between the two modes. Compared with the similar biasing mechanism used in [31], the proposed exchangeable biasing method can be gracefully compatible with the parallel/series mismatch-resilient QB-DPA.

In summary, through mode reconfiguration and biasing-setting reciprocity, the unique capability of mismatch recovery of the QB-DPA architecture can be extended to a wideband implementation. Meanwhile, with proper OMN and coupler coordination to absorb the device parasitics and minimize the phase offset, a high back-off and peak efficiency are assured over the wide operational bandwidth. This proposed reconfigurable broadband capacitively QB-DPA platform, is the first-ever developed LM PA that against the wideband dynamic mismatch through simply reconfiguration of voltage bias control (main/auxiliary settings and open/short for isolation port).

III. Prototype Design and Demonstration

In this section, based on the proposed theory, the practical design methodology is presented to achieve wideband and mismatch-resilient QB-DPA. The prototype is designed using GaN devices (CGH40006P) targeting for a frequency range from 1.7 to 2.7 GHz. In this realistic design, the parallel QB-DPA is configured as the primary mode at matched condition, while the reconfiguration to series mode is triggered at certain mismatch conditions.

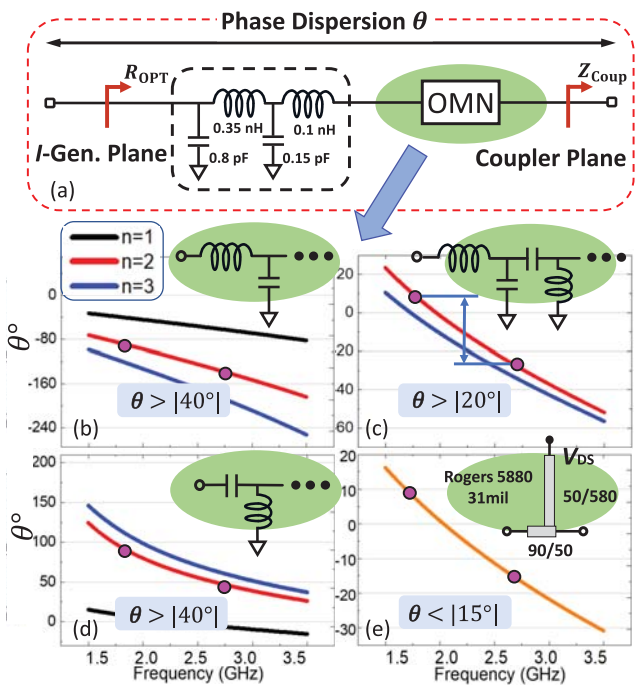

Fig. 8. Analysis of the wideband OMNs and phase dispersion from current source plane to coupler plane. (a) Concept of OMN design, (b) low-pass OMN, (c) low-pass plus high-pass OMN, (d) high-pass OMN, and (e) proposed OMN.

A. Design of Wideband Matching Network

For the wideband QB-DPA OMN design, the fundamental goal is to achieve optimal matching quality for Doherty LM over the target bandwidth and meanwhile minimize the phase dispersion. Fig. 8(a) describes the generic OMN of the QB-DPA architecture. The selected CGH 40006P devices' package parasitics are extracted and modeled based on [32]. To design the wideband OMN, a variety of matching networks are investigated. In Fig. 8(b)–(d), the conventional multistage with different number (n) of stages low-pass and high-pass networks as well as their hybrid combination are designed together with the parasitics to perform an ideal impedance transformation from coupler plane ($Z_{\text{Coup.}}$) to intrinsic I-generator plane (R_{OPT}). For the OMN with only low-pass or high-pass, a two-stage design leads to a large phase dispersion of $|\theta| > 40°$ over the entire frequency range, which is not suitable for achieving the desired Doherty performance according to the mathematical analysis in Section II-B. The two-stage OMN with hybrid low-pass/high-pass design also yields an unwanted phase dispersion of $|\theta| > 20°$ at the higher half of the target frequency range.

On the other hand, it is discovered that the single-stage high-pass or low-pass OMN can offer the minimized phase dispersion. Thus, a quasi-single-stage OMN is proposed with a simple biasing line acting as a shunt inductor and a series tuning TL in Fig. 8(e). The proposed OMN can effectively compensate for the parasitics across the operational bandwidth, and it can meanwhile offer a good matching quality over the target bandwidth in conjunction with the characteristic impedance of quadrature coupler $Z_{\text{Coup.}}$. Realistically, the three-section

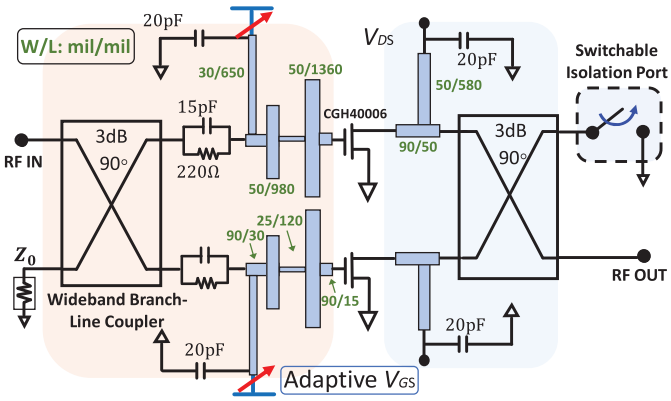

Fig. 9. Full Schematic of the designed wideband mismatch-resilient QB-DPA architecture.

wideband quadrature coupler is designed with an arbitrary real impedance, and the output port can be transformed to Z_0 with an wideband matching network. In this design with the 6-W GaN transistors, $Z_{\text{Coup.}}$ is finally designed to $Z_0 = 50\ \Omega$ as the optimal value. As depicted in Fig. 8(e), the overall phase offset θ from intrinsic I-generator plane to coupler plane is maintained within the tolerable range of $\theta < 15°$ to result in a wideband Doherty performance. It is important to point out that this parasitics compensation methodology is generally applicable for different GaN transistors with similar parasitic networks by adjusting the design parameters [27], [33]. For the high-power PAs with a low optimal resistance $R_{\text{OPT}} < 50\ \Omega$, the impedance transformation can be primarily provided by the quadrature coupler [34]. Thus, this "single-element" matching technique is capable to maintain a low-phase dispersion for any $R_{\text{OPT}} < 50\ \Omega$.

It is worthy to note that the overall OMN of the main/auxiliary paths are designed identically for mode reconfiguration that ensures a consistent QB-DPA performance between parallel and series modes in terms of $\text{OP}_{1\,\text{dB}}$, gain, efficiency, and linearity profile (AM/AM and AM/PM) [21], [25]. Meanwhile, by means of the symmetrical topology, the phase delays of main and auxiliary paths are automatically equalized at the saturation power level, leading to the maximized power combining efficiency. The same wideband coupler is designed at the input side together with a two-stage low-pass input matching [35] transforming the 50-Ω across target bandwidth. It is noted that the wideband quadrature coupler can also be realized in many ways, e.g., using slow wave structure as study in [36] for a miniaturized size and decent loss performance. To stabilize the designed QB-DPA architecture, both an RC network in series with the transistor and a resistor at the gate bias feed line are placed at main and auxiliary paths. Thereafter, the entire circuit is cosimulated with the transistors, components, and electromagnetic models of layout using Keysight ADS. The full circuit schematic is presented in Fig. 9 with all the circuit parameters illustrated.

B. Exchangeable Biasing for Multiband Operation and Parallel/Series Reconfiguration Against Load Mismatch

The output matching and combiner networks set the foundation for the wideband QB-DPA architecture, while the

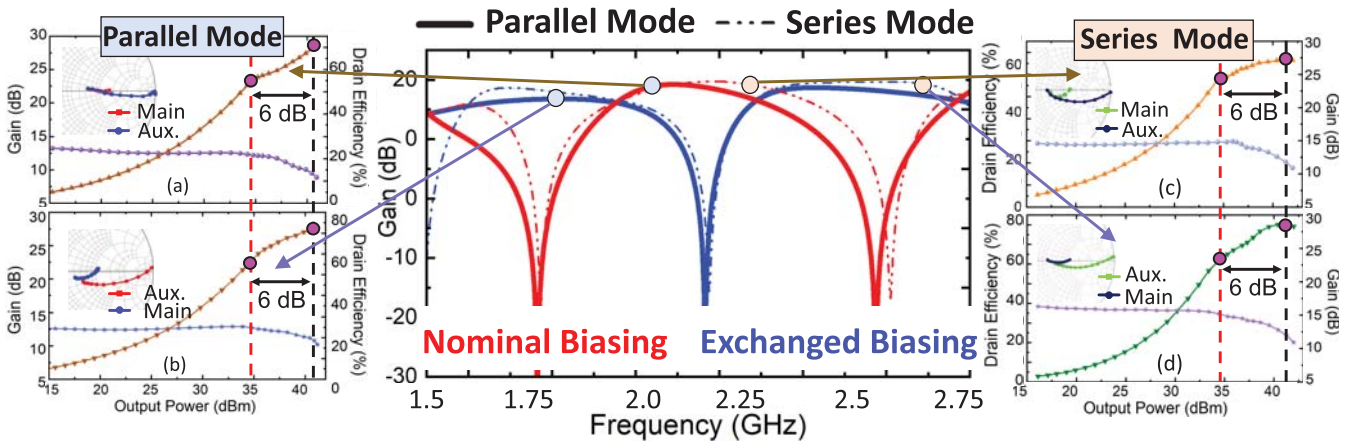

Fig. 10. Small-signal and large-signal simulation results for wideband QB-DPA in (a) and (b) parallel and (c) and (d) series modes and with nominal/exchanged biasing.

reconfiguration between parallel and series modes and nominal and exchanged biasing is the key enabler to allow simultaneously broadband operation and mismatch resilience. Practically, the alternation between parallel and series QB-DPA can be realized through exchanging gate biasing and switching the isolation-port loading of output coupler by an RF switch. Meanwhile, the reciprocal reconfiguration between nominal-exchanged biasing is simply realized by swapping the role of main and auxiliary PAs within a single QB-DPA mode, e.g., the primary parallel mode. In the previous research [21], [25], the RF switch design and implementation at the isolation port for mode reconfiguration has been thoroughly elaborated, which is not repeated in this work. Thus, the switching from parallel to series mode in this prototype demonstration is performed by manually placing a bypass capacitor at the isolation port of output quadrature coupler.

The wideband performance of designed QB-DPA is first investigated at matched load condition. Fig. 10 presents the small-signal and large-signal simulations with both parallel and series modes. The small-signal S_11 in the middle plot of Fig. 10 clearly illustrates a complementary frequency response with nominal and exchange biasing settings, which is observed for both parallel and series modes. In large-signal simulation, a desired DPA LM (on the inset Smith Chart) and efficiency profile are shown around the center frequency with nominal biasing, as shown in Fig. 10(a). Through exchanging the roles of main auxiliary amplifiers, the rest of operational bandwidth can be covered as illustrated by the gain, efficiency and load trajectory behaviors in Fig. 10(b), which perfectly reflects the complementary responses of the reciprocal biasing. The same complementary large-signal results are also simulated for series mode at the center and edge frequencies as shown in Fig. 10(c) and (d). Further, under load mismatch of 2:1 VSWR, the QB-DPA is simulated for parallel and series modes at 2.1 and 2.6 GHz, respectively. Fig. 11 summarized the results for comparison. For parallel mode at 2.1 GHz shown in Fig. 11(a) and (b), using the same bias setting as used in the 50-Ω condition, the QB-DPA suffers from clearly degradation of $OP_{1\,dB}$ and efficiency (both at $OP_{1\,dB}$ and 6-dB back-off). However, through reconfiguration, a nearly consistent $OP_{1\,dB}$

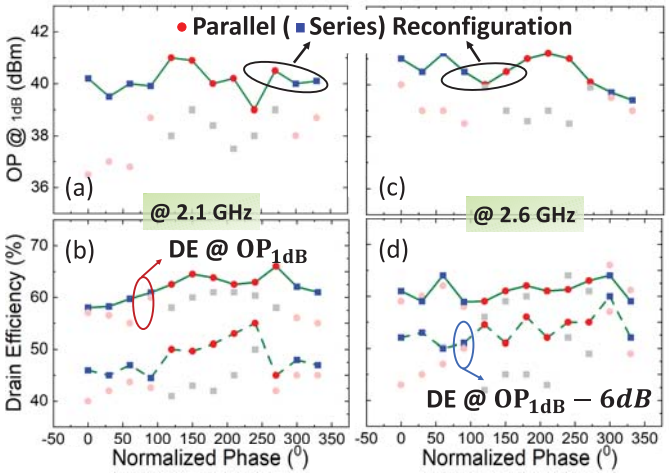

Fig. 11. Simulation performance of wideband QB-DPA under 2:1 VSWR for $OP_{1\,dB}$ and DE at $OP_{1\,dB}$ and 6-dB back-off region for (a) and (b) at 2.1 GHz and (c) and (d) at 2.6 GHz.

of the DPA (39.2–40.9 dBm) is achieved over the entire VSWR circle, and the drain efficiency (DE) at $OP_{1\,dB}$ and 6-dB back-off efficiency are improved to >59% and >45.6%, respectively. It is interesting to point that the operational impedance regions for parallel and series modes calculated in theory (i.e., $|z_L| > 1$ for parallel and $|z_L| < 1$ for series) is still valid in the simulation. This mismatch recovery feature is demonstrated at 2.6 GHz as well in Fig. 11(c) and (d).

In the above design, the gate-biasing voltages are set depending on both the operational frequency (nominal biasing for mid band and exchanged biasing for band edges) and mismatched load condition (parallel for $|z_L| > 1$ and series for $|z_L| < 1$). Moreover, with the minimized phase dispersion of wideband matching networks, the simulation results well agree with the design equations described in Section II-B.

IV. Fabrication and Measurement Results

The designed circuit schematic is electromagnetically modeled using ADS Momentum simulator and cosimulated with active components to optimize the overall performance.

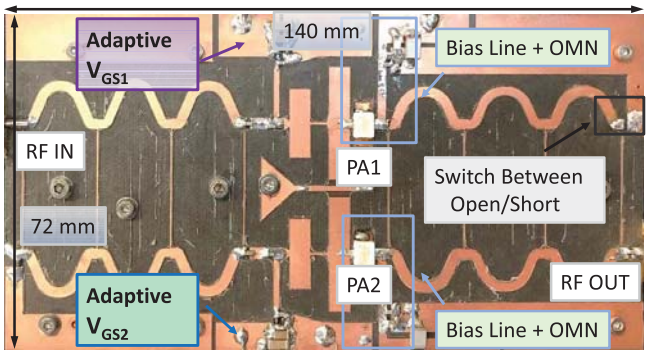

Fig. 12. Top view of the fabricated PCB board.

The prototype QB-DPA is shown in Fig. 12 which is fabricated on the Rogers 5880 substrate with 31-mil thickness. Considering parallel QB-DPA as the primary mode, at the center frequency, PA2 is set as the main cell with V_{GS} to −2.9 V in class-AB, while PA1 is operated as the auxiliary cell with gate bias of −4.8 V in class-C. The gate bias voltages of two PAs are exchanged and reoptimized experimentally at different frequencies and modes. The drain voltage is 28 V for both PAs. To experimentally verify the QB-DPA's wideband operation and mismatch-resilience, the designed QB-DPA is evaluated with both the continuous waveform and modulated signal, respectively.

A. Continuous-Wave Measurement

In the CW measurement, a single-tone power-swept input signal is generated to measure the QB-DPA performance at different power levels with a standard matched load impedance of 50-Ω. As the results shown in Fig. 13, a maximum efficiency of 58%–62% is measured at $OP_{1\,dB}$ with the nominal biasing setting from 2.0 to 2.3 GHz, together with a 48%–51% back-off efficiency at 6-dB output back-off (OBO). To cover the rest of the operational bandwidth, the main and auxiliary gate bias voltages are swapped in the exchanged setting. Meanwhile, the measured peak efficiency is within a range of 56%–78% over the complementary frequencies with the corresponding 6-dB OBO efficiency varying from 47%–67% as presented in Fig. 14. The PAE is presented as well with dot-line in Fig. 13 for the corresponding frequency. A clearly Doherty behavior is observed over the in-band frequencies that attributes to the nominal/exchanged biasing scheme. Further, a flat gain profile and 39.1–40.8-dBm output power are obtained at $OP_{1\,dB}$ in both biasing settings with the operation bandwidth extended from 1.6 to 2.7 GHz, which are in good agreement with the simulation results in Fig. 10. Due to the symmetry, the CW measurement of series mode is not discussed here, while it will be performed in mismatched-load condition.

Next, to demonstrate the load-mismatch tolerance of QB-DPA architecture, the designed QB-DPA is further evaluated with a CW stimulus over the 2:1 VSWR circle beginning from 1.7 GHz. The illustrative configuration of measurement setup is shown in Fig. 15. A driver amplifier (ZHL-5W-422+) provides sufficient input power, which is followed by an isolator. Two directional couplers are used to accurately sample and measure the input and output power. The DUT

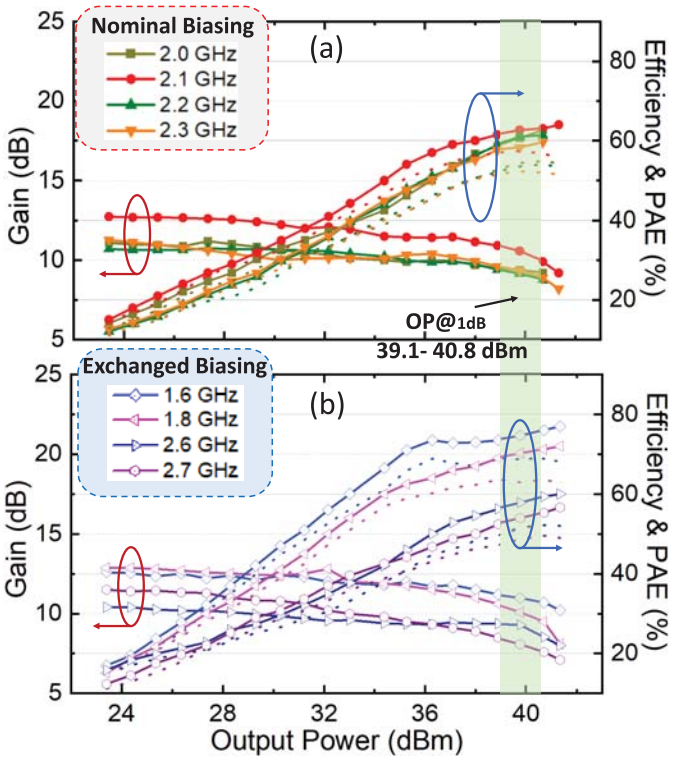

Fig. 13. CW measurement of power-swept DE, PAE, and gain over1.6–2.7 GHz at matched-load condition for parallel QB-DPA with (a) nominal and (b) exchanged biasing.

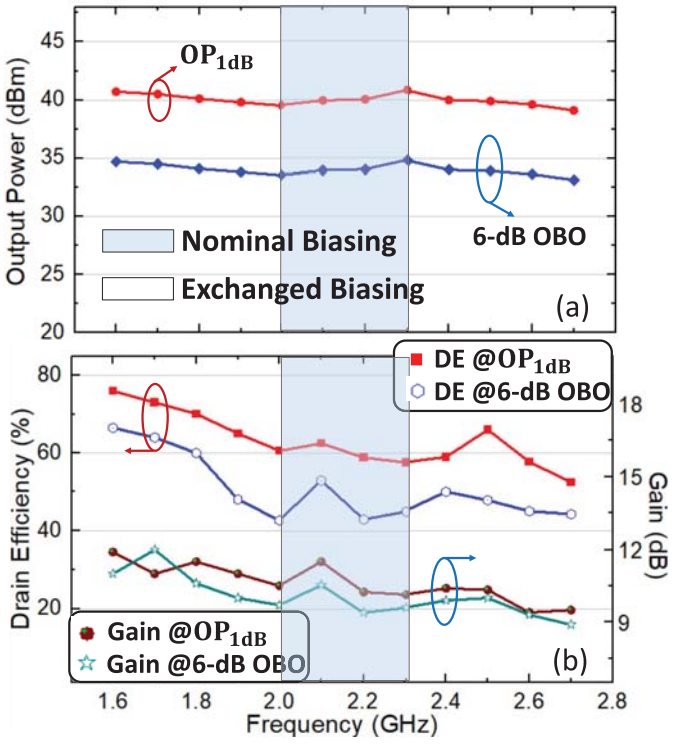

Fig. 14. Frequency response with exchangeable biasing for (a) output power and (b) DE and gain.

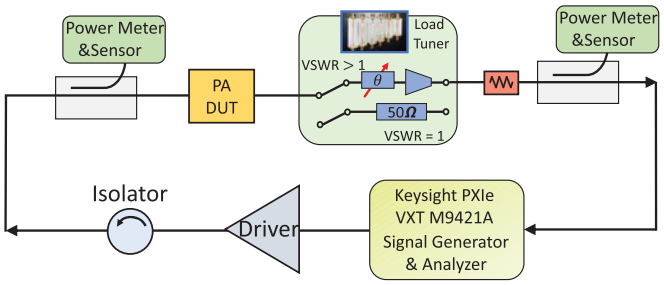

Fig. 15. Measurement setup for characterization of the wideband QB-DPA under nominal 50-Ω and mismatched loading (VSWR > 1) conditions.

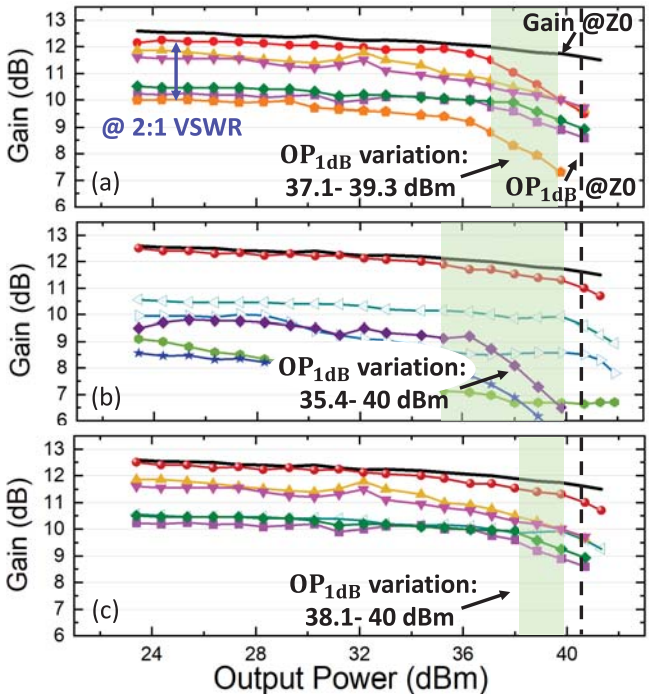

Fig. 16. Measured $OP_{1\,dB}$ over 2:1 VSWR with CW signal at 1.7 GHz. (a) Parallel only. (b) Series only. (c) Reconfiguration combination.

output is connected to a mismatched load which is swept over the entire 2:1 VSWR circle using a delay line with variable length (swept from 0° to 180°) together with an 2:1 impedance transformer. Finally, a Keysight PXIe vector transceiver (VXT M9421) is used as CW/modulated signal generator and analyzer. Both parallel and series modes are test under the mismatch. The series QB-DPA mode is activated by connecting the isolation port to ground through a 20-pF RF bypass capacitor together with the gate biases swapped from parallel mode. As shown in Fig. 16 a single-mode QB-DPA suffers from excessive compression and AM–AM nonlinearity for both the parallel/series modes, in which the gain profiles are extracted with the different phase points on the 2:1 VSWR circle. Specifically, for parallel mode only, the $OP_{1\,dB}$ variation is around 2.2 dB over 360° VSWR phases, and it is even worse for series mode where the gain variation can be as high as 4.6 dB. Nevertheless, through reconfiguration, a much more converged response with a nearly consistent $OP_{1\,dB}$ of 38.1–40 dBm is achieved over the full span of 2:1 VSWR.

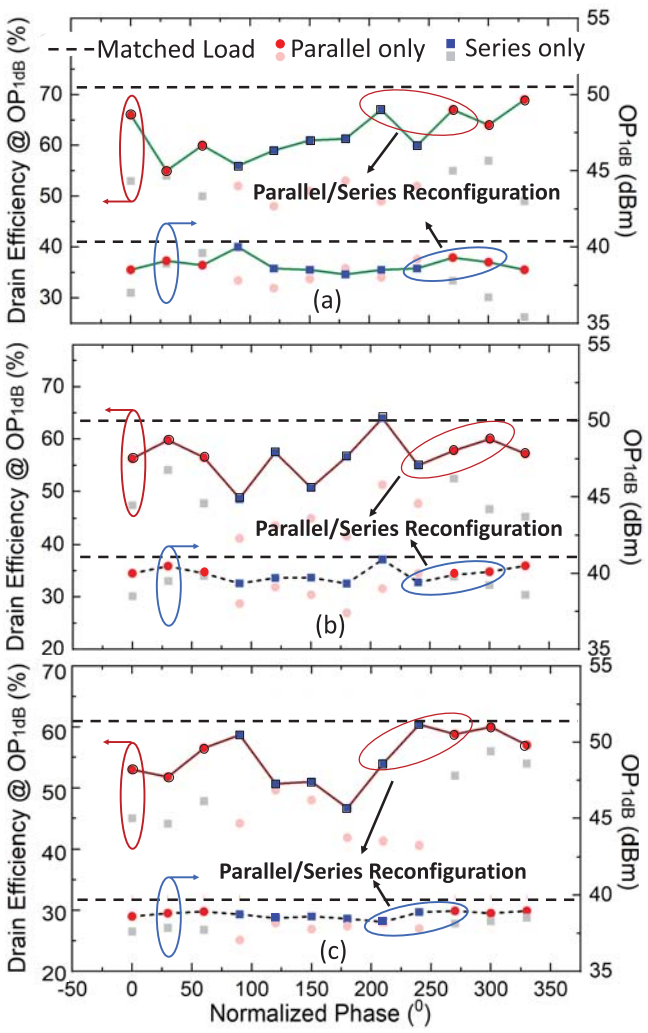

Fig. 17. Measured DE and $OP_{1\,dB}$ over 2:1 VSWR with CW signal at (a) 1.7, (b) 2.1, and (c) 2.6 GHz.

Then, the recovery capability of QB-DPA is further characterized at different frequencies in terms of the efficiency and P_{out} at 1-dB compression points under the same 2:1 VSWR load mismatch. At center frequency 2.1 GHz in Fig. 17(b), the efficiency at $OP_{1\,dB}$ can be significantly improved over the entire 2:1-VSWR circle through modes reconfiguration with a well-maintained consistent $OP_{1\,dB}$ between 39.1 and 40.5 dBm. Similar efficiency improvement and P_{out} recovery are measured at low-edge frequency 1.7 GHz and the high-edge side 2.6 GHz with mode reconfiguration as well. It is important to point out that the AM-AM and AM-PM can be distorted due to the load mismatch. Therefore, certain fine adjustment of biasing is needed to reoptimize the linearity of the dedicated DPA mode at different frequencies and load conditions. The above results clearly validate the wideband mismatch-recovery capability of the proposed QB-DPA technology.

B. Modulated Measurement

Similarly, the modulated measurement is started with the matched 50-Ω load condition at parallel mode. The

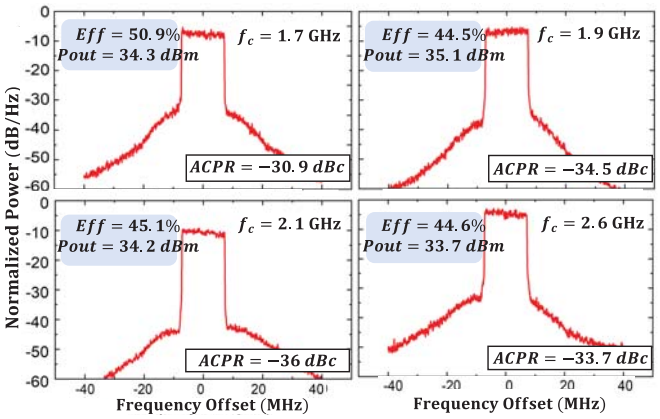

Fig. 18. Modulation measurement under 20-MHz 64-QAM LTE signal over 1.7–2.6 GHz with 50-Ω load.

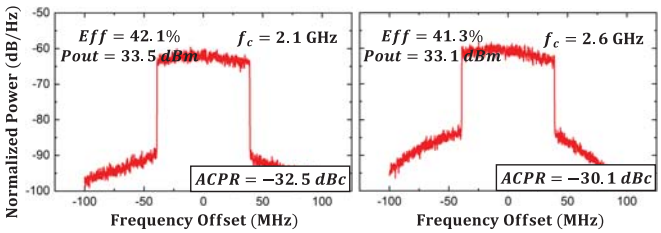

Fig. 19. Modulation measurement under 80-MHz 5G-NR with 50-Ω load.

dynamic performance, i.e., efficiency and linearity of the wideband QB-DPA, is first evaluated under 20-MHz modulation bandwidth using a single-carrier 64 QAM long-term evolution (LTE) signal with 9.6-dB PAPR. The measured power spectral density (PSD) and adjacent channel power ratio (ACPR) are depicted in Fig. 18 with various in-band frequencies are obtained. The lowest achievable ACPR is down to −36 dBc at the center frequency (2.1 GHz) without DPD applied. For the higher frequency where exchanged biasing triggered, the QB-DPA achieves an raw ACPR of −33.7 dBc with 44.6% efficiency at an average P_{out} of 33.7 dBm. A comparable efficiency, P_{out} and ACPR can be obtained for the lower in-band frequencies (1.7 and 1.9 GHz). A wideband 5G-NR 80-MHz modulated signal is characterized at center 2.1 GHz with nominal bias and exchanged the bias for 2.6 GHz as well. The proposed QB-DPA achieves average efficiency of 42.1%, and 41.3% with <−30.1-dBc ACPR around 33.1-dBm average P_{out} in Fig. 19.

The designed QB-DPA is further evaluated with single-carrier 64-QAM 20-MHz bandwidth modulated signal under load VSWR 2:1 at 2.1 GHz to demonstrate the recovery of mismatch-induced degradation. The QB-DPA is tested with four symmetrical impedance points in Smith Chart on the 2:1 VSWR circle. It should be noted that impedance points, Z_{A-D}, plotted in Fig. 20 are calibrated to the output port of the quadrature coupler. The measured P_{out}, efficiency, ACPR, and error vector magnitude (EVM) are presented for comparison. Specifically, at Z_A point, an inductive load with normalized impedance larger than 1 (i.e., $|z_L| > 1$), the ACPR and EVM can be recovered when configured at parallel mode, with the average efficiency at 42.9% and P_{out} equals 33.1 dBm.

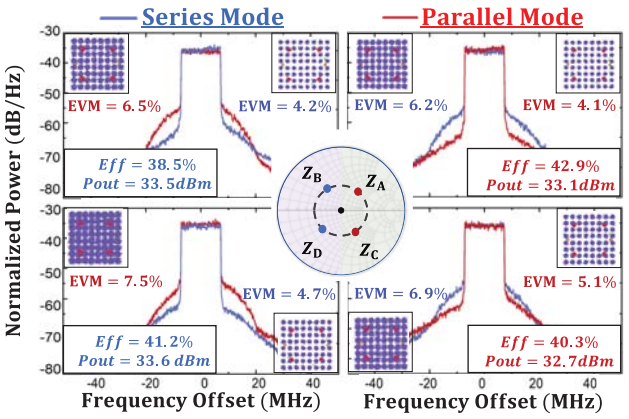

Fig. 20. Measured ACPR, EVM, P_{OUT} and average efficiency over 2:1 VSWR with 64-QAM 20-MHz bandwidth signal at 2.1 GHz.

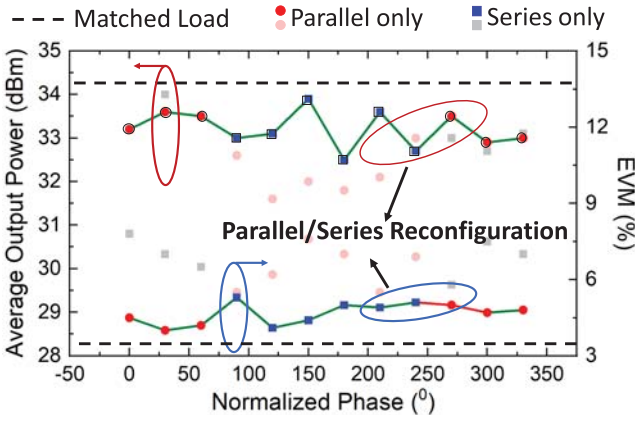

Fig. 21. Modulated evaluation using 64-QAM 20-MHz bandwidth 4G LTE signal at 2:1 VSWR at 2.1 GHz for average P_{OUT} and EVM.

While for Z_B, where the normalized impedance $|z_L| < 1$, the QB-DPA at parallel mode suffers from severely impairment of EVM and ACPR, which aligns with the degraded $\text{OP}_{1\,\text{dB}}$ observed in Fig. 11. In contrast, with parallel/series reconfiguration, the linearity-related specs are significantly improved with comparable achieved P_{out} and efficiency for both modes. Moreover, this effect can be validated for the capacitive loads (e.g., Z_C and Z_D) across the lower half part of the Smith chart as well. Similar to CW load mismatch measurement, the modulated EVM and average P_{out} can be significantly recovered versus load phase mismatch in Fig. 21, where the QB-DPA is characterized over 2:1 VSWR at −31-dBc ACPR (5.3% EVM). Through above CW and modulation measurements, the proposed QB-DPA achieves the competitive capability to restore the EVM, maintain a stable $\text{OP}_{1\,\text{dB}}$ and largely recover the efficiency when subjected to the load mismatch across the target bandwidth. In this design, the goal is to present the concept of wideband mismatch-resilient DPA, which is not targeted for any specific wireless standards. Thus, this article focuses on obtaining the best in-band performance specs, such as P_{out}, PAE and EVM.

Table I summarizes the state-of-the-art of wideband QB-DPA compared to other mismatch-resilient PAs published recently. Besides its competitive achievements with 50-Ω load, the proposed PA demonstrates a wideband VSWR resilience

TABLE I
COMPARISON WITH STATE-OF-THE-ART OF RECENTLY-REPORTED MISMATCH-RESILIENT PAS

Ref.	This Work				[17] TMTT-2021		[18] JSSC-2020		[20] TMTT-2021		[21] TMTT-2021		[23] TMTT-2021	
Technology	GaN-PCB				CMOS		CMOS		GaN-PCB*		GaN-PCB		LDMOS-PCB	
Freq (GHz)	1.7-2.7				26-42		39		3.6		3.5		0.9	
Load (Z_0/VSWR)	50Ω	2:1 @1.7GHz	2:1 @2.1GHz	2:1 @2.6GHz	50Ω	4:1**	50Ω	3:1	50Ω	2:1	50Ω	2:1	50Ω	2:1
$\mathbf{OP_{1dB}}$ (dBm)	39.1-40.8‖	38.1-40	39.1-40.2	37.8-39.2	19.2	17.2*	20.2	18.5-19.1	43.5	42.6-43.4	40.7	38.8-40.4	29.4	29-29.6
$\mathbf{DE\ @OP_{1dB}}$ (%)	58-78	—	49-62	46-61	24†	16.5	33.3†	20.6-25.3	68§	54-64	68.4§	51-59	59.1§	46.5-61.3
Modulation Signal	64-QAM 20MHz				64-QAM 2GHz		64-QAM 3Gb/s		LTE 5MHz		64-QAM 20MHz		64-QAM 3.8MHz	
PAPR	9.6				—		—		5.5		9.6		6	
$\mathbf{P_{out}}$ (dBm)	33.7-35.1	32.6-33.9 @2.1 GHz			9.8	—	12.2	> 11.2	—		35	33-34.2	22	21.9-22.1
$\mathbf{DE_{avg}}$ (%)	44.5-50.9	38.1-42.9 @2.1 GHz			10.2†		16.1†	> 9.6	46.4	40.2-43	45	32.5-42.5	24.4	21-23
ACPR (dBc)	-36	-31 @2.1 GHz			-25		-25.4	< -22.8	-31.8	< -30.1	-41	—	-48	-45

*Graphically estimated ** Measured at one frequency ‖ At center frequency † PAE § Peak efficiency

across the full span of 2:1 VSWR circle for the first time. Specifically, for the CW measurement, this design exhibits <1.9-dB output power variation and >46% efficiency at $OP_{1\,dB}$ over the designed bandwidth at 2:1 VSWR. Meanwhile, comparing with the DPAs in [20] and [21] using similar technology as in this design, the proposed QB-DPA achieves <1.4-dB variation P_{out} and <−31-dBc ACPR with modulation signal under mismatch, while maintaining a comparable average efficiency. Further, compared with other contemporary narrowband mismatch-resilient PAs [17], [18], [23], the designed QB-DPA still largely recovers the ACPR, average efficiency, and reduces the P_{out} fluctuation, again well verifying the proposed theory.

V. CONCLUSION

In this article, a mode-reconfigurable QB-DPA platform is proposed for the first time with concurrent wide bandwidth and VSWR resilience. It presents a comprehensive theoretical analysis on the effects of OMN's phase dispersion on QB-DPA, the practical design of OMN to minimize the overall phase dispersion, and an exchangeable biasing scheme, all of which set the foundation for implementing broadband QB-DPAs. Meanwhile, the broadband design methodology well cooperates with the series/parallel reconfiguration that extends the operational frequency range of QB-DPA's mismatch resilience. A wideband QB-DPA prototype using GaN technology is designed and developed to verify the proposed concept ranging from 1.7 to 2.7 GHz. In the case with standard 50-Ω load, the CW experimental results exhibit a 56%–78% efficiency at $OP_{1\,dB}$ and 47%–71% 6-dB OBO efficiency, respectively. Driven with a 20-MHz LTE modulated signal with 9.6-dB PAPR, the measured PA achieves 44%–51% average efficiency over the operation bandwidth and up to −36-dBc ACPR at matched load condition together with a −32.5-dBc ACPR achieved with 80-MHz 5G-NR signal. Moreover, when the PA loading is under 2:1 VSWR, the designed QB-DPA can maintain a minimal variation of $OP_{1\,dB}$ and gain as well as high linearity (EVM/ACPR) and average efficiency across the target bandwidth. For the realistic application scenarios, the output signal and the load impedance are sensed real time, and certain iterations by algorithms (searching for an optimal combination of DPA mode and gate biasing) can be performed to autonomously reconfigure the QB-DPA states. Alternatively, more cost-effective ways can be invented to reconfigure the PAs in the entire array. This is an emerging research area that falls out of the scope of this manuscript. Overall, the proposed wideband mismatch-resilient QB-DPA offers a compelling solution to realize a spectrum-efficient and performance-robust PA in MIMO system.

REFERENCES

[1] D. M. Pozar, "A relation between the active input impedance and the active element pattern of a phased array," *IEEE Trans. Antennas Propag.*, vol. 51, no. 9, pp. 2486–2489, Sep. 2003.

[2] C. Fager, X. Bland, K. Hausmair, J. C. Cahuana, and T. Eriksson, "Prediction of smart antenna transmitter characteristics using a new behavioral modeling approach," in *IEEE MTT-S Int. Microw. Symp. Dig.*, Jun. 2014, pp. 1–4.

[3] L. Savy and M. Lesturgie, "Coupling effects in MIMO phased array," in *Proc. IEEE Radar Conf. (RadarConf)*, May 2016, pp. 1–6.

[4] T. L. Marzetta, E. G. Larsson, H. Yang, and H. Q. Ngo, *Fundamentals of Massive MIMO*. Cambridge, U.K.: Cambridge Univ. Press, 2016.

[5] E. Bjornson, L. Van der Perre, S. Buzzi, and E. G. Larsson, "Massive MIMO in sub-6 GHz and mmWave: Physical, practical, and use-case differences," *IEEE Wireless Commun.*, vol. 26, no. 2, pp. 100–108, Apr. 2019.

[6] X. Chen, S. Zhang, and Q. Li, "A review of mutual coupling in MIMO systems," *IEEE Access*, vol. 6, pp. 24706–24719, 2018.

[7] C. Fager, T. Eriksson, F. Barradas, K. Hausmair, T. Cunha, and J. C. Pedro, "Linearity and efficiency in 5G transmitters: New techniques for analyzing efficiency, linearity, and linearization in a 5G active antenna transmitter context," *IEEE Microw. Mag.*, vol. 20, no. 5, pp. 35–49, May 2019.

[8] S. C. Cripps, "RF power amplifiers for wireless communications," *IEEE Microw. Mag.*, vol. 1, no. 1, p. 64, Mar. 2000.

[9] K. Hausmair *et al.*, "Prediction of nonlinear distortion in wideband active antenna arrays," *IEEE Trans. Microw. Theory Techn.*, vol. 65, no. 11, pp. 4550–4563, Nov. 2017.

[10] F. M. Barradas, P. M. Tomé, J. M. Gomes, T. R. Cunha, P. M. Cabral, and J. C. Pedro, "Power, linearity, and efficiency prediction for MIMO arrays with antenna coupling," *IEEE Trans. Microw. Theory Techn.*, vol. 65, no. 12, pp. 5284–5297, Dec. 2017.

[11] K. Hausmair, P. N. Landin, U. Gustavsson, C. Fager, and T. Eriksson, "Digital predistortion for multi-antenna transmitters affected by antenna crosstalk," *IEEE Trans. Microw. Theory Techn.*, vol. 66, no. 3, pp. 1524–1535, Mar. 2018.
[12] X. Wang, Y. Li, C. Yu, W. Hong, and A. Zhu, "Digital predistortion of 5G massive MIMO wireless transmitters based on indirect identification of power amplifier behavior with OTA tests," *IEEE Trans. Microw. Theory Techn.*, vol. 68, no. 1, pp. 316–328, Jan. 2020.
[13] T. W. Barton, J. Gordonson, and D. J. Perreault, "Transmission line resistance compression networks for microwave rectifiers," in *IEEE MTT-S Int. Microw. Symp. Dig.*, Jun. 2014, pp. 1–4.
[14] D. Ji, J. Jeon, and J. Kim, "A novel load mismatch detection and correction technique for 3G/4G load insensitive power amplifier application," *IEEE Trans. Microw. Theory Techn.*, vol. 63, no. 5, pp. 1530–1543, May 2015.
[15] Y. Yoon *et al.*, "A 2.4-GHz CMOS power amplifier with an integrated antenna impedance mismatch correction system," *IEEE J. Solid-State Circuits*, vol. 49, no. 3, pp. 608–621, Mar. 2014.
[16] C. F. Gonçalves, F. M. Barradas, P. M. Cabral, and J. C. Pedro, "Switch-based variable length stubs network for PA load sensitivity reduction," *IEEE Access*, vol. 7, pp. 152576–152584, 2019.
[17] C. R. Chappidi, T. Sharma, and K. Sengupta, "Multi-port active load pulling for mm-wave 5G power amplifiers: Bandwidth, back-off efficiency, and VSWR tolerance," *IEEE Trans. Microw. Theory Techn.*, vol. 68, no. 7, pp. 2998–3016, Jul. 2020.
[18] N. S. Mannem, M.-Y. Huang, T.-Y. Huang, and H. Wang, "A reconfigurable hybrid series/parallel Doherty power amplifier with antenna VSWR resilient performance for MIMO arrays," *IEEE J. Solid-State Circuits*, vol. 55, no. 12, pp. 3335–3348, Dec. 2020.
[19] C. F. Gonçalves, F. M. Barradas, L. C. Nunes, P. M. Cabral, and J. C. Pedro, "Dynamic supply voltage control for PA output power correction under variable loading scenarios," *IEEE Trans. Microw. Theory Techn.*, vol. 69, no. 1, pp. 745–755, Jan. 2021.
[20] C. F. Gonçalves, F. M. Barradas, L. C. Nunes, P. M. Cabral, and J. C. Pedro, "Quasi-load insensitive Doherty PA using supply voltage and input excitation adaptation," *IEEE Trans. Microw. Theory Techn.*, vol. 70, no. 1, pp. 779–789, Jan. 2022.
[21] H. Lyu, Y. Cao, and K. Chen, "Linearity-enhanced quasi-balanced Doherty power amplifier with mismatch resilience through series/parallel reconfiguration for massive MIMO," *IEEE Trans. Microw. Theory Techn.*, vol. 69, no. 4, pp. 2319–2335, Apr. 2021.
[22] H. Lyu and K. Chen, "Wideband quasi-balanced Doherty power amplifier with reciprocal main/auxiliary setting and mismatch-resilient parallel/series reconfiguration," in *IEEE MTT-S Int. Microw. Symp. Dig.*, Jun. 2021, pp. 736–739.
[23] G. D. Singh, H. M. Nemati, and L. C. N. de Vreede, "A low-loss load correction technique for self-healing power amplifiers using a modified two-tap six-port network," *IEEE Trans. Microw. Theory Techn.*, vol. 69, no. 9, pp. 4069–4081, Sep. 2021.
[24] G. R. Nikandish, R. B. Staszewski, and A. Zhu, "Unbalanced power amplifier: An architecture for broadband back-off efficiency enhancement," *IEEE J. Solid-State Circuits*, vol. 56, no. 2, pp. 367–381, Feb. 2021.
[25] H. Lyu and K. Chen, "Balanced-to-Doherty mode-reconfigurable power amplifier with high efficiency and linearity against load mismatch," *IEEE Trans. Microw. Theory Techn.*, vol. 68, no. 5, pp. 1717–1728, May 2020.
[26] D. M. Pozar, *Microwave Engineering*, 3rd ed. Hoboken, NJ, USA: Wiley, 2005.
[27] Y. Cao, H. Lyu, and K. Chen, "Asymmetrical load modulated balanced amplifier with continuum of modulation ratio and dual-octave bandwidth," *IEEE Trans. Microw. Theory Techn.*, vol. 69, no. 1, pp. 682–696, Jan. 2021.
[28] G. Lv, W. Chen, Y. Zhang, N. Chen, F. M. Ghannouchi, and Z. Feng, "A highly linear GaN MMIC Doherty power amplifier based on phase mismatch induced AM–PM compensation," *IEEE Trans. Microw. Theory Techn.*, vol. 70, no. 2, pp. 1334–1348, Feb. 2022.
[29] X. Fang, A. Chung, and S. Boumaiza, "Linearity-enhanced Doherty power amplifier using output combining network with predefined AM–PM characteristics," *IEEE Trans. Microw. Theory Techn.*, vol. 67, no. 1, pp. 195–204, Jan. 2019.
[30] A. Grebennikov, "Power combiners, impedance transformers and directional couplers: Part III," *High Freq. Electron.*, vol. 7, pp. 42–52, Mar. 2008.
[31] M. Li, J. Pang, Y. Li, and A. Zhu, "Ultra-wideband dual-mode Doherty power amplifier using reciprocal gate bias for 5G applications," *IEEE Trans. Microw. Theory Techn.*, vol. 67, no. 10, pp. 4246–4259, Oct. 2019.
[32] Wolfspeed Products, Durham, NC, USA. *6-W RF Power GaN HEMT*. Accessed: Mar. 2020. [Online]. Available: https://www.wolfspeed.com/cgh40006/
[33] H. Lyu and K. Chen, "Hybrid load-modulated balanced amplifier with high linearity and extended dynamic range," *IEEE Microw. Wireless Compon. Lett.*, vol. 31, no. 9, pp. 1067–1070, Sep. 2021.
[34] Y. Cao, H. Lyu, and K. Chen, "Continuous-mode hybrid asymmetrical load-modulated balanced amplifier with three-way modulation and multi-band reconfigurability," *IEEE Trans. Circuits Syst. I, Reg. Papers*, vol. 69, no. 3, pp. 1077–1090, Mar. 2022.
[35] K. Chen and D. Peroulis, "Design of highly efficient broadband class-E power amplifier using synthesized low-pass matching networks," *IEEE Trans. Microw. Theory Techn.*, vol. 59, no. 12, pp. 3162–3173, Dec. 2011.
[36] Y. Cao and K. Chen, "Highly miniaturized and wideband 3-dB quadrature hybrid using slow-wave coupled line," in *IEEE MTT-S Int. Microw. Symp. Dig.*, Jun. 2021, pp. 247–250.

Haifeng Lyu (Graduate Student Member, IEEE) received the bachelor's degree in electrical engineering and automation from the Chengdu University of Technology, Chengdu, China, in 2010, and the master's degree in electrical engineering from The University of Rhode Island, Kingston, RI, USA, in 2017. He is currently pursuing the Ph.D. degree at the University of Central Florida, Orlando, FL, USA.

His research interests include novel highly efficient and linear power amplifier (PA) architectures and reconfigurable RF/mm-Wave circuits.

Mr. Lyu was a recipient of the First Place Award of the High Efficiency Power Amplifier Student Design Competition (HEPA-SDC) in the IEEE MTT-S International Microwave Symposium (IMS) 2020 and 2021, consecutively. He was a recipient of the Second Place and Third Place Award of HEPA-SDC in 2022 and 2019 IMS, respectively. He was the First Place Winner of the Carrier Aggregation BAW Quadplexer Module Design Competition in IMS 2019. He was also a recipient of the Second Place Award of Student Paper Competition in IEEE WAMICON 2019.

Kenle Chen (Senior Member, IEEE) received the bachelor's degree in communication engineering from Xi'an Jiaotong University, Xi'an, China, in 2005, the master's degree in electronics and information engineering from Peking University, Beijing, China, in 2008, and the Ph.D. degree in electrical engineering from Purdue University, West Lafayette, IN, USA, in 2013.

As a Graduate Researcher at Purdue University from 2008 to 2013, he made significant contributions in high-efficiency broadband power amplifiers and codesign of reconfigurable RF circuits for smart communication systems. From 2013 to 2015, he was a Principal/Lead RFIC Engineer with innovational startups, where he led the research and development of multiple successful products of CMOS integrated power amplifiers and frontend solutions for the latest WLAN platforms, e.g., IEEE802.11ac/ax. Prior to his career in academia, he has extensive experiences in wireless and semiconductor industries. From 2015 to 2017, he was a Staff RFIC Engineer with Skyworks Solutions, Inc., Irvine, CA, USA, where he focused on the development of RF frontend modules for the advanced smart-phone platforms. He was an Assistant Professor with The University of Rhode Island, Kingston, RI, USA, for one year. In 2018, he joined the University of Central Florida, Orlando, FL, USA, where he is currently an Assistant Professor with the Department of Electrical and Computer Engineering. His research interests include energy-efficient, wideband, and ultrahigh-speed RF/mm-Wave circuits and systems for 5G-and-beyond communications, extreme-performance power amplifiers in CMOS and compound semiconductor technologies, reconfigurable RF/mm-Wave electronics, and innovational wireless radio concepts/architectures/applications.

Dr. Chen was a recipient of the 2012 IEEE Microwave Theory and Techniques Society (MTT-S) Graduate Fellowship. He was also a recipient of the High Efficiency Power Amplifier Design Competition in the IEEE MTT-S International Microwave Symposium (IMS) from 2011 to 2012, consecutively. He is an Associate Editor of the IEEE TRANSACTIONS ON MICROWAVE THEORY AND TECHNIQUES.